Rock Mechanics and Rock Engineering
https://doi.org/10.1007/s00603-024-03868-9

TECHNICAL NOTE

Modal Analysis of a Lava Tube Roof Complex: Tabernacle Hill, Utah, USA

Guglielmo Grechi[1,2] · Jeffrey R. Moore[2] · Erin K. Jensen[2] · Molly E. McCreary[2] · Theresa L. Czech[2] · Madeleine M. Festin[2]

Received: 5 June 2023 / Accepted: 14 March 2024
© The Author(s) 2024

Highlights

- We used array-based ambient vibration modal analysis and eigenfrequency modeling to characterize the dynamic behavior and structural conditions of a partly collapsed lava tube roof.
- Multiple resonance modes were identified from spectral and cross-correlation analyses, and used to calibrate a heterogeneous numerical model of the lava tube.
- Our study shows that the combination of experimental and numerical modal analysis is a valuable tool for mapping and structural characterization of underground cavity roofs.

Keywords Modal analysis · Ambient vibrations · Numerical modeling · Structural health monitoring · Underground cavities

1 Introduction

Near-surface underground cavities can pose significant hazards when located near urban areas or strategic infrastructure. Generally, the combination of local geology and anthropogenic factors can lead to the formation of sinkholes, geologic features often originating from dissolution and deep piping processes (Waltham 2008; Esposito et al. 2021), which can evolve toward collapse of the ground surface. At the same time, underground cavities, such as caves, caverns, and lava tubes, can also be designated as natural or cultural heritage sites known for their unique geological features and archeological value (Nehme et al. 2013; Woo et al. 2019; Bentivenga et al. 2019). The UNESCO World Heritage List currently includes more than 100 natural and anthropic cavern sites worldwide famous for their natural and historical significance. Thus, improved knowledge of the location, spatial extent, and structural conditions of underground cavities is increasingly needed for both hazard and conservation management, including design of restoration or mitigation strategies to avoid potential safety threats or heritage losses (Cardarelli et al. 2006; Esposito et al. 2021).

Traditional invasive methods of cavity detection, such as drilling, trenching and field surveys offer high-resolution geological data but are often time-consuming, costly, and limited in coverage (Liu et al. 2023). To overcome these challenges, geophysical methods and remote sensing techniques have emerged as valuable tools for the non-invasive location of underground cavities. Among geophysical methods, electrical resistivity tomography (ERT) (Cardarelli et al. 2006; Park et al. 2014), ground penetrating radar (GPR) (Ebraheem and Ibrahim 2019; Pilecki et al. 2021), microgravity (Arisona et al. 2023), and seismic methods (Liang et al. 2018; Rao et al. 2021) have been widely applied to investigate karst networks, sinkholes, and underground instabilities (Liu et al. 2023). Satellite-based monitoring techniques, such as Interferometric Synthetic Aperture Radar (InSAR), have also succeeded in detecting cavities and monitoring the evolution of sinkholes and subsidence-prone areas, demonstrating the ability to provide wide spatial data coverage with adequate geometric and temporal resolution (Malinowska et al. 2019; Esposito et al. 2021). However, selecting the appropriate investigation technique represents

✉ Guglielmo Grechi
guglielmo.grechi@uniroma1.it

[1] Department of Earth Sciences, Sapienza University of Rome, Rome, Italy

[2] Department of Geology and Geophysics, University of Utah, Salt Lake City, UT, USA

Published online: 26 April 2024

a nontrivial issue as it often involves a trade-off between geometric resolution, cost-effectiveness, and diagnostic capabilities (Cardarelli et al. 2014).

A significant shortcoming of the abovementioned techniques is their limited ability to retrieve information on the structural conditions of underground cavities. While most geophysical or remote sensing techniques are generally employed for mapping cavity networks, structural characterization of potential ground instabilities is mainly conducted using geomechanical testing and invasive field surveying techniques (Margherita et al. 2018; Bastidas et al. 2022). Nevertheless, recent studies have highlighted that ambient vibration modal analysis can be used to reveal mechanical and dynamic material properties of ground and slope instabilities, as well as their extent and structure, by identifying natural resonance frequencies, local site amplifications and polarization attributes (Kleinbrod et al. 2019; Bessette-Kirton et al. 2022; Geimer et al. 2022). In particular, the combination of experimental modal analysis and numerical eigenfrequency modeling has been used to improve geologic models by constraining material properties (Moore et al. 2018; Geimer et al. 2020; Müller and Burjánek 2023) and has provided valuable new insights on local boundary conditions and structural characteristics (Colombero et al. 2017; Bessette-Kirton et al. 2022).

In this study, we utilize an integrated approach comprising ambient vibration measurements and numerical modeling to analyze the modal behavior of a partly collapsed lava tube roof complex in the Tabernacle Hill volcanic field of central Utah. We generated data from a dense nodal geophone array consisting of 43 stations to perform spectral and array cross-correlation analyses to identify and visualize resonance modes of the roof complex. Results from experimental modal analysis were used to calibrate a heterogeneous 3D finite-element numerical model of the site. The combination of numerical modeling and array cross-correlation ultimately improved our geologic model of the site by providing a refined mechanical and structural characterization of the lava tube roof complex. These outcomes can be used as the basis for future analyses or monitoring, and the approach is applicable across a wide variety of similar applications and sites.

2 Study Area

The Tabernacle Hill lava field is located in central Utah, USA, within the Black Rock Desert volcanic district and precisely the Ice Spring Quaternary volcanic field (age < 100–0.7 ka) (Johnsen and Smith 2010). The Tabernacle Hill volcano erupted ~ 16 ka ago into Lake Bonneville during the high-stand phase of the Provo level (Oviatt 1991), beginning its activity as a phreatomagmatic eruption that generated a primary tuff cone. Subsequent eruptions generated cinder cones, basaltic and andesitic lava flows, a lava lake, and a dense field of lava tubes (Hintz 2008; Johnsen and Smith 2010). This site is now a tourist attraction in the Fillmore, UT region due to the presence of easily accessible lava tubes, which can have diameters up to 15 m and several windows or skylights (i.e., partly collapsed portions of the lava tube roof) (Fig. 1a). These windows have openings between 1 and 10 m, while the lava tube roof has a variable thickness of 0.5–1 m (Fig. 1b–d). We selected the site due to its excellent and safe access in order to test the feasibility of an integrated geophysical and numerical approach for modal analysis and structural characterization of underground cavity roofs.

The outcropping basalt at the site is vesicular with a relatively large volume of gas pockets and corresponding rough texture. From field observations, the rock mass is generally massive and poorly layered apart from the lava tube roof and window areas which feature dense fracture networks with open joints, often 1–10 mm wide and characterized by weathered infilling and diffuse surface alteration. Based on these characteristics and the blocky to very blocky rock mass joint density, which can also be inferred by the size of the collapsed blocks covering the lava tube floor, we rate the Geological Strength Index (GSI) at the site as between 45 and 55 (Hoek et al. 2013). This GSI range is comparable to what has been observed and measured at other lava tube sites (Theinat et al. 2020). Due to the impossibility of collecting intact rock core samples at the site, we relied on literature values to characterize rock matrix material properties for the implementation in our numerical modeling (Goodman 1989; Schultz 1993). The size and geometric features of the lava tube interior were measured and reconstructed using a LiDAR scan performed inside the underground cavity (Fig. 1e). A detailed description of the reconstruction stages of the lava tube 3D model is provided below.

3 Methods

Ambient vibrations were recorded by 43 three-component Fairfield Zland 5-Hz nodal geophones during an overnight survey in October 2022. The array, which covered an area of 700 m^2, consisted of five lines (L1–L5) spaced ~ 5 m apart, with 3-m station spacing, and was designed to encompass the extent of the curving lava tube (Fig. 2a). Two additional sensors (namely stations 998 and 999) were deployed to improve coverage in the skylight area between alignments L4 and L5. Geophones were leveled and aligned to magnetic north. Due to the presence of rocky topsoil, most geophones far from the window areas were deployed using the attached spikes, while sensors closer to the collapsed roof were adhered to bedrock using adhesive putty (i.e., stations

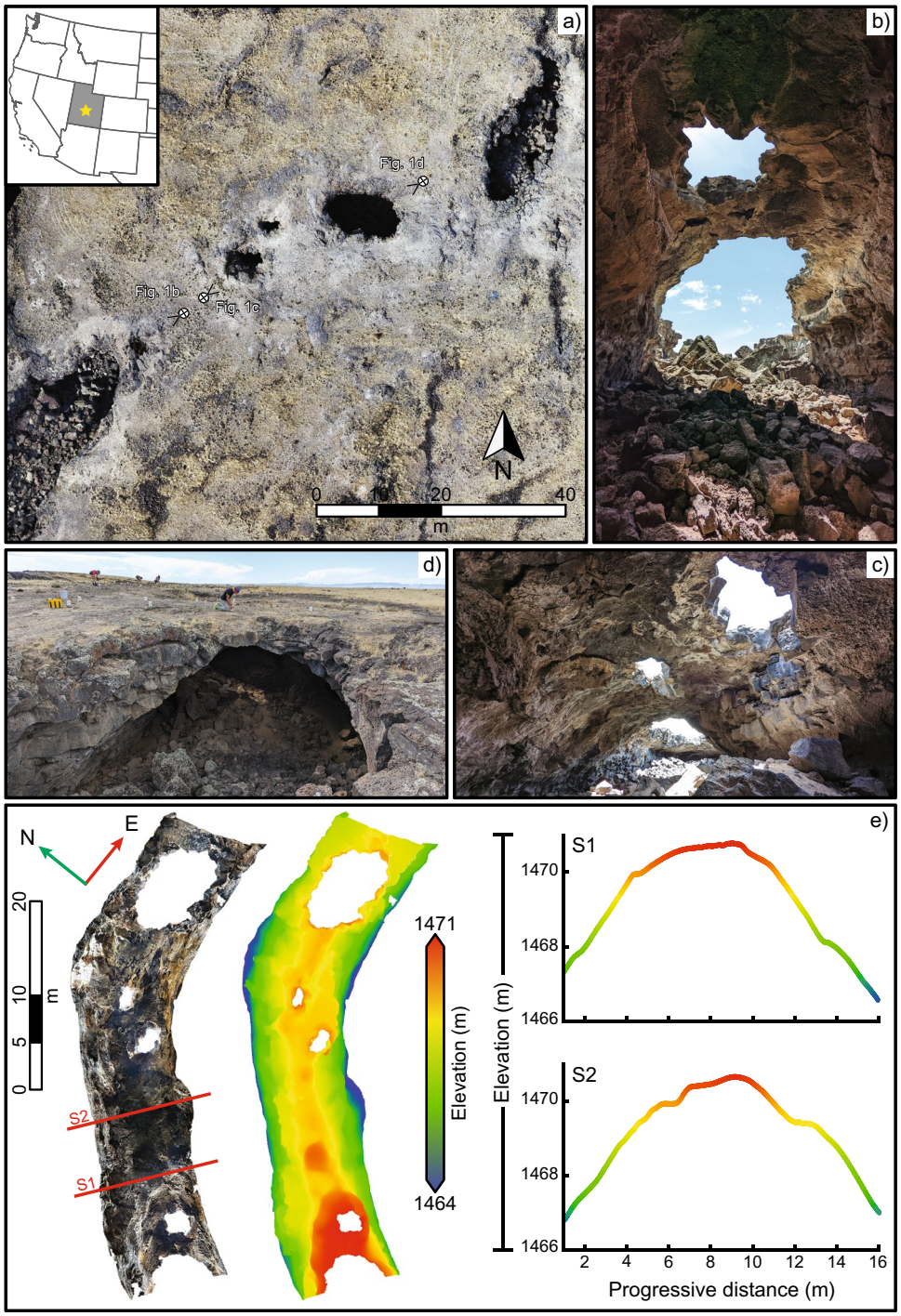

Fig. 1 **a** Aerial view of the Tabernacle Hill lava tube site located near Fillmore, UT, USA (location inset). **b**, **c** Photos of the main windows or skylights from the SW to **d** the NE sector of the investigated lava tube (person for scale; see photo locations in (**a**). **e** 3D model and DEM of the lava tube interior constructed from the LiDAR survey also showing topographic cross sections at S1 and S2

104, 105, 106, 506, 998, 999). We additionally deployed one nodal geophone underground inside the lava tube in the NE section of the array as a local reference for surface stations (white triangle in Fig. 2a).

We recorded continuous ambient vibration data at a sampling rate of 250 Hz for 18 h between 9 October 22:00 UTC (16:00 MST) and 10 October 16:00 UTC (08:00 MST). Vibration data were processed for spectral content to identify natural frequencies of the lava tube roof complex. Prior to processing, the dataset was examined to extract the longest undisturbed (e.g., due to wind, earthquakes, or anthropogenic noise) continuous time block. We selected a 40-min window (10 October 2022 01:30–02:10 UTC) of quiet conditions for all further processing. We first removed the mean, linear trend and the instrument response for every component of each array station. Power spectral densities (PSD) were then computed using Welch's method (Welch 1967) using 40-s Hanning-tapered windows with 75% overlap

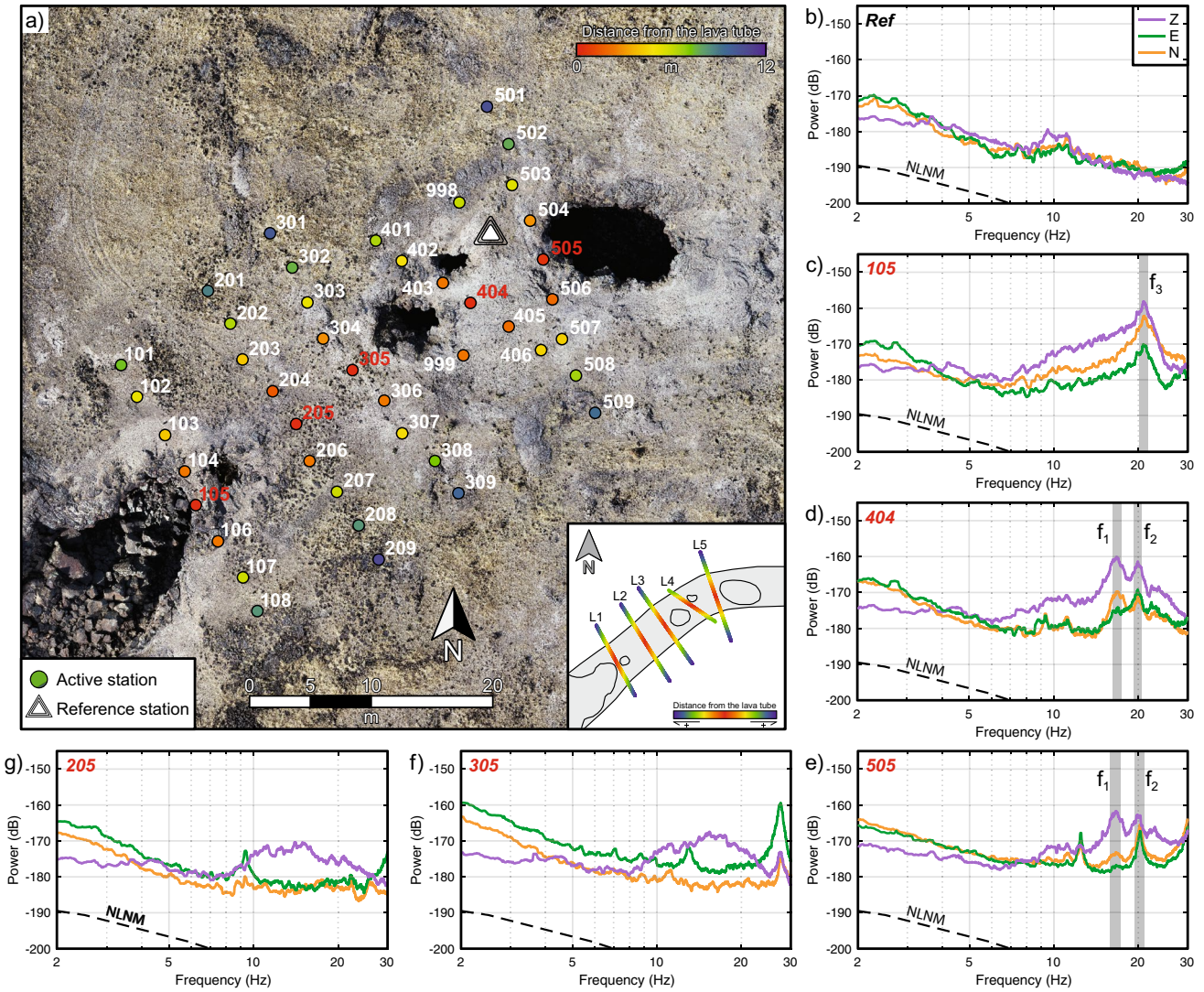

Fig. 2 **a** Aerial view of the Tabernacle Hill lava tube with the location of surface active (colored circles) and underground reference (white triangle) geophone array stations. Surface stations are color coded by distance from the lava tube central axis. The inset sketch shows the spatial distribution of the five geophone lines with respect to the lava tube outline and window locations. **b**–**g** Velocity power spectral density estimates for the reference and five active geophone stations. Decibel powers are relative to 1 m^2 s^2 Hz^{-1}. Gray shadings in **c**–**e** highlight three resonance modes identified across the array

and a 0.15 Hz smoothing window. Poor ground coupling at some stations resulted in high noise levels on horizontal components, which led to us excluding three stations from further analysis (stations 207, 302 and 506). Therefore and because of the anticipated modal deflections, we elected to focus solely on analysis of vertical component recordings. Spectral ratios of vertical components across the array were computed using the station inside the lava tube as a local reference (Colombero et al. 2018; Finnegan et al. 2022). We first inspected the reference time series and PSD to ensure it was suitably free from spurious noise. We then calculated the amplitude spectrum of every station segmenting the recordings into 100-s Hanning-tapered windows with 80% overlap and a 0.2 Hz smoothing window. Spectral ratios were computed for every segment by dividing each roof station spectra by the reference spectra and then averaged over the 40-min window. Lastly, we constructed mean vertical spectral ratio maps using nearest neighbor interpolation to generate 2D visualizations of the spatial distribution of amplified ground motion in 0.5 Hz frequency bands.

Experimental modal analysis was performed via cross-correlation using 40 of the 43 roof stations to characterize the spatial distribution of relative modal displacements. All data were first downsampled to 100 Hz, segmented into 5-min tapered windows with linear trend and mean values removed (Geimer et al. 2020; Bessette-Kirton et al. 2022), and spectral whitening was applied (Bensen et al. 2007; Lin et al. 2013). The maximum amplitude of every window was

used for temporal normalization before stacking each station pair to retrieve cross-correlograms for vertical components (ZZ). Every station pair cross-correlogram was filtered to 0.3 Hz bandwidth windows between 5 and 23 Hz, and the zero-time lag amplitude for each station pair was extracted omitting auto-correlations (Geimer et al. 2020; Bessette-Kirton et al. 2022). The resulting curves allowed us to identify the relative amplitude and phase at each array station, enabling visualization of mode shapes along individual lines or across the array. Every station curve was normalized by the maximum Root Mean Square amplitude (RMS) of all station curves and averaged to obtain mean and standard deviation values used to reconstruct mode shapes. We then extracted mean amplitude values at all station locations and for every previously identified resonance frequency, and plotted these as vectors on a 3D model of the area to visualize mode shapes across the array.

We performed 3D finite-element eigenfrequency modeling to support structural and material characterization of the lave tube roof complex. To accurately recreate the geometry, we generated a georeferenced drone-based photogrammetric model of the roof area using the Structure-from-Motion (SfM) software Bentley Context Capture (bentley.com), while the scaled inner geometry of the lava tube was reconstructed using the LiDAR sensor of an Apple iPhone 13 Pro with the open-source 3D Scanner App (3dscannerapp.com). Reconstruction of the lava tube inner geometry, as well as the possibility of measuring its width, height and roof thickness at the skylight areas was crucial for accurate model construction. The availability of a LiDAR scan, in particular, enabled the generation of a 3D model reflecting the in situ conditions of the lava tube by preserving the most important geometric features. Moreover, it allowed us to approximate the overall detailed geometry of the lava tube using a more regular, circular-shaped tunnel with 5 m radius to avoid computational issues due to large geometric complexities. The two meshes were then merged using Meshmixer (meshmixer.com), refined to smooth surfaces and eliminate irregularities, before being transformed into a solid 3D object that we imported into COMSOL Multiphysics (comsol.com) for eigenfrequency analysis. Based on the results of spectral analysis, we cropped the model to preserve the geophone array coverage by removing areas not participating in modal deformation. The final model, which includes three skylights and the ~ 40 m long lava tube, was created by applying automatic meshing with tetrahedral and triangular finite elements (i.e., 78,000 elements) characterized by maximum and minimum side lengths ranging from 2.5 and 0.1 m. Hence, we adopted two different numerical representations of the lava tube under the assumption of homogeneous density (ρ) and Poisson's ratio (ν), at a nominal value for basalt of 2900 kg/m^3 and 0.25, respectively (Schultz 1993, 1995). In a first modeling attempt, we simulated the entire lava tube area as an isotropic, continuous and homogeneous rock medium. We assigned the entire model a Young's modulus (E) of 3 GPa, which was calibrated by matching the first measured resonance frequency of the site. Next, based on field observations and considering both local rock mass conditions and the presence of collapsed parts of the roof complex (i.e., skylights), we implemented a heterogeneous model allowing variable Young's moduli for different areas of the lava tube roof complex. In particular, we assigned a reduced Young's modulus (E_r) in the window areas as compared to the surrounding uncollapsed roof. Fixed boundary conditions were applied to replicate in situ conditions (Fig. 4a). We then varied E of the window areas to match the identified resonance frequencies and relative modal displacements from experimental data analysis (Moore et al. 2018; Geimer et al. 2020).

4 Results

Spectral analysis of array data revealed elevated spectral peaks on station alignments L1, L4, and L5, which we identify as the first three resonance frequencies: $f_1 = 17.1$ Hz, $f_2 = 19.3$ Hz, $f_3 = 20.8$ Hz (Fig. 2b–g). These peaks are spatially clustered in the northeast and southwest sectors of the lava tube roof and were not identified at all array stations. Only stations close to the windows, which were themselves generated by localized collapses of the lava tube, show clear spectral peaks. In particular, the first two resonance frequencies have maximum spectral amplitudes at central stations of L4 and L5 (i.e., stations 404 and 505) (Fig. 2d–e), while the third emerges only on L1 (i.e., station 105) (Fig. 2c). No corresponding peaks are found at the reference station or on other alignments, suggesting that the identified frequencies can be interpreted as resonance modes of different sectors of the roof complex.

Computed spectral ratios using the station inside the lava tube as a reference showed vertical amplifications of up to 60 on alignments in the window areas (L1, L4, L5; Fig. 2a). Spectral ratios for all stations in L1, L4 and L5 are shown in Fig. 3a–c. Spectral ratio peaks match those observed from PSD plots, supporting the hypothesis that these represent resonance modes of the lava tube roof. Moreover, the amplitude of spectral ratios along each alignment decreases markedly with distance from the lava tube center. For example at L1, the closest stations to the window (i.e., 104, 105 and 106) have peak amplification at f_3 ranging from 20 to 60, while all other stations show no amplification (Fig. 3a). This same behavior can be observed for L4 and L5 at f_1 and f_2 (Fig. 3d–e). Here, a few additional higher-order peaks are visible on L4 and L5 at > 22 Hz, especially on stations 405, 503 and 504, however, these may be artifacts related to the computation of spectral ratios as they do not appear on corresponding PSDs. High spectral amplification recorded at f_1

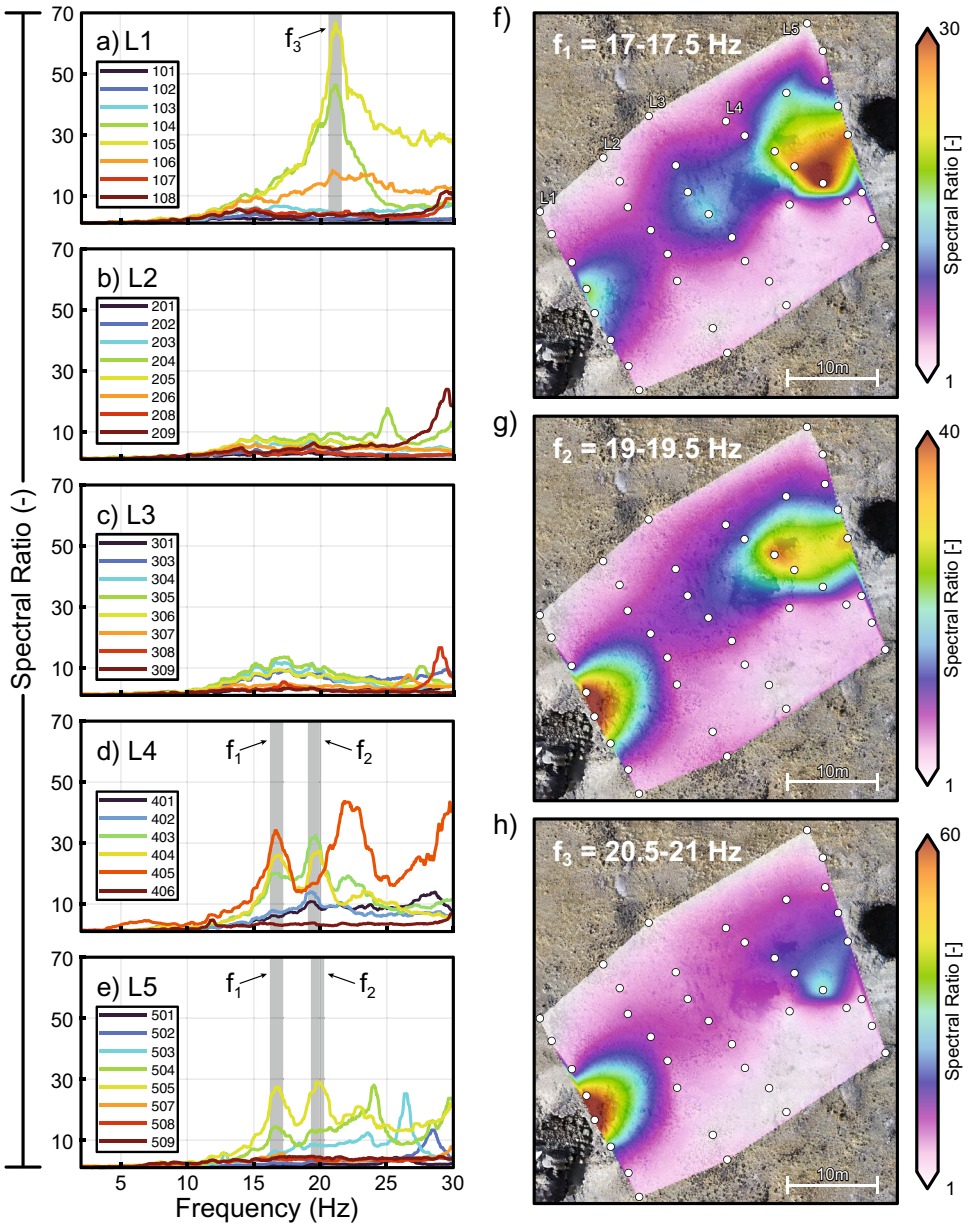

Fig. 3 **a-e** Average vertical spectral ratios for geophone alignments L1–L5. Gray shadings indicate frequency bands corresponding to the first three resonance modes of the roof complex that were considered for computation of spectral ratio maps **f**–**h**. For each spectral ratio map, the color scale is normalized by the maximum amplification value recorded across the array to enhance visualization of the different modes. Station locations are indicated by white circles

near station 405 was interpreted as caused by poor ground coupling of the geophone rather than deriving from local structural conditions. This same hypothesis led to us neglecting three other stations from our analysis since they showed PSD and spectral ratios that were not comparable to surrounding stations (i.e., stations 207, 302 and 506).

We generated interpolated vertical spectral ratio maps to visualize the spatial distribution of amplification across the array for each of the identified resonance frequencies (Fig. 3f–h). Each frequency is characterized by clear spatial clustering of amplified motion, with maximum amplitudes in the window areas of the roof complex. The first two modes are limited to the NE sector of the lava tube, where three of the four windows are closely concentrated, while the third is located around the small bridge bounding the window in the SW (Fig. 1b). This zonation is particularly visible by the abrupt decay of spectral ratios far from the window areas and at the lava tube perimeter, both in the transverse and longitudinal directions. For instance, considering the map for f_3 (Fig. 3 h), spectral ratios drop from 64 to 1 within a distance of 15 m moving from the window to the farthest stations of L1.

Cross-correlation analysis revealed relative modal displacements for each of the identified resonance frequencies, enabling the description of mode shapes and relative phase across the array. Results for L1 at f_3 (20.8–21.1 Hz) are shown in Fig. 4b. Relative displacements describe a vertical bending mode mainly affecting stations near the window

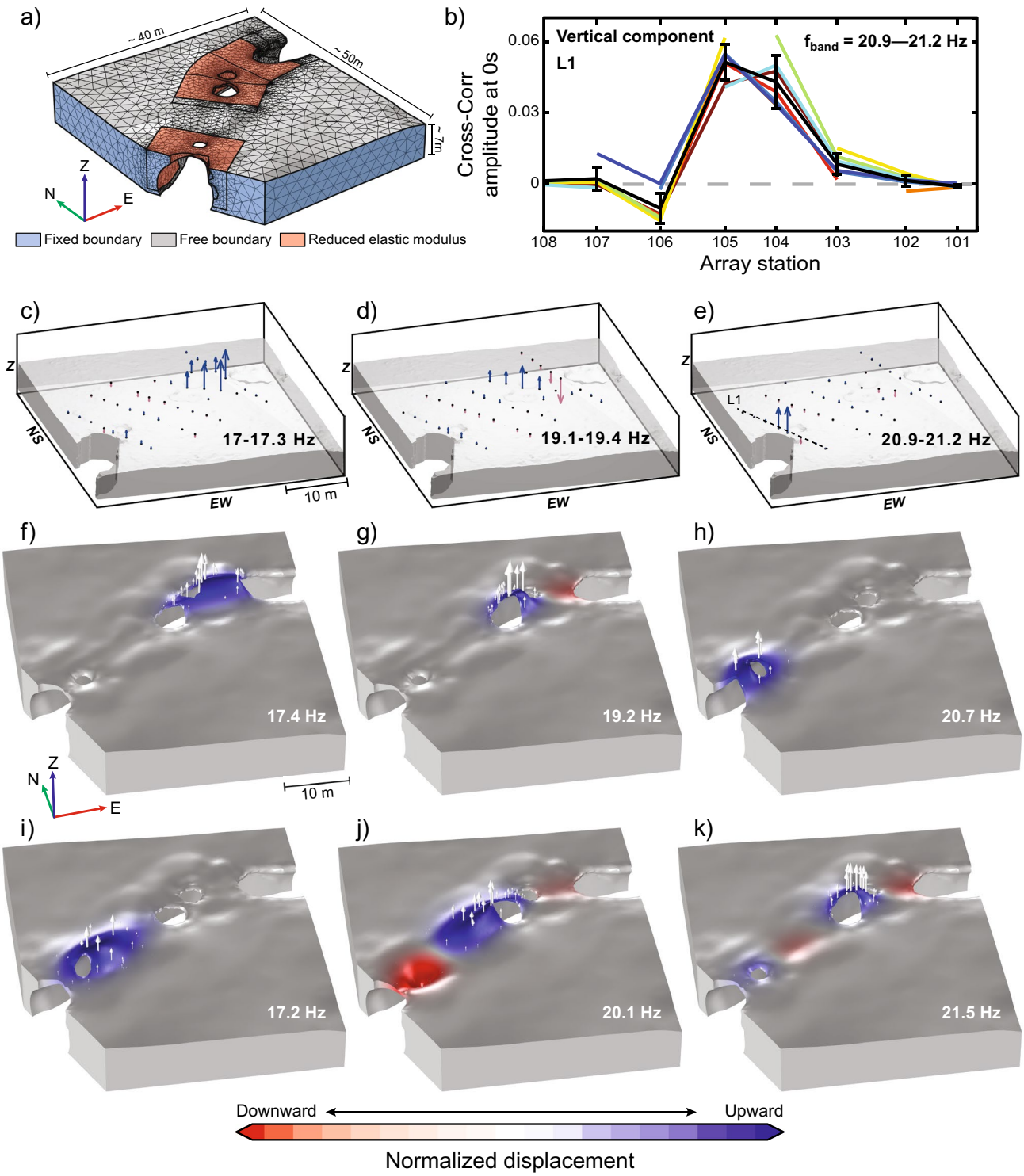

Fig. 4 Results of experimental and finite-element modal analysis. **a** 3D visualization of the mesh implemented in COMSOL highlighting window areas with reduced Young's modulus (E_r). **b** Array cross-correlation results for line L1 in the 20.9–21.2 Hz frequency band corresponding to the third identified resonance mode (f_3) of the roof complex. Colored lines represent the RMS-normalized cross-correlation amplitude at each station with respect to all other stations, while the black line shows the mean and standard deviation. **c**–**e** 3D representation of normalized modal displacement vectors at each array station for the three identified resonance frequencies (Figs. 2, 3). Red and blue arrows indicate upward and downward modal displacement, respectively. **f**–**h** Modelled resonance modes of the lava tube for the heterogeneous model including reduced elastic modulus volumes. **i**–**k** Modelled resonance modes of the lava tube for the homogeneous model. For both models, normalized modal displacement amplitude and direction are described by colors and arrows

(i.e., 104 and 105). To better constrain the spatial distribution of modal displacements, we plotted vertical-component cross-correlation results on a 3D model (Fig. 4c–e). The resulting maps demonstrate that relative displacements for the identified resonance modes agree with the pattern of amplification retrieved from spectral ratio analysis. The spatial visualization of modal vectors also provides phase information for each of the resonance modes, which is not available from spectral ratios. Such information is particularly valuable as it helps distinguish different mode shapes for f_1 and f_2, which are close in frequency and located in the same area of the array, depicting a first- and second-order vertical bending mode in the NE sector of the roof complex at f_1 and f_2, respectively (Fig. 4c–d).

We used the experimental description of the first three resonance modes of the lava tube to calibrate a numerical eigenfrequency model. We first implemented a homogeneous and isotropic model to reproduce the modal parameters obtained from experimental results. Under this assumption, however, modeled resonance frequencies and mode shapes poorly matched experimental results, indicating that a homogeneous model is inappropriate for the site (Fig. 4i-k). For this reason, and to account for the structural setting of the area, we generated a heterogeneous model by assigning a reduced Young's modulus (E_r) to the partly collapsed sections of the lava tube (i.e., window areas) in contrast to the intact portions of the roof (Fig. 4a). This model allowed us to achieve a good fit between field data and numerical modeling results, closely matching eigenfrequencies and mode shapes for the three identified resonance modes (Fig. 4f–h). This match was achieved by assigning a reduced Young's modulus of 2.4 GPa for the partly collapsed window areas as compared to 10 GPa in the intact areas. Furthermore, the numerical modeling results predict predominantly vertical displacement vector fields at all three resonance frequencies, validating our simplification of analyzing only the vertical component of geophone data at each array station.

5 Discussion and Conclusion

We analyzed a dense, array-based ambient vibration dataset to characterize the modal behavior of a partly collapsed lava tube roof. Results revealed the spectral and polarization properties (i.e., frequency, ground motion amplification and orientation) of three resonance modes of the roof in the frequency range between 16 and 21 Hz. The localized spatial distribution of modal deformation (Figs. 3, 4) indicates that local geo-structural features of the lava tube play a key role in controlling its dynamic behavior. We found that resonance modes are only observable in the NE and SW sectors of the lava tube around partly collapsed roof areas. Field observations indicate that thickness of the roof complex is almost constant over the study area, with minimal variations moving from collapsed to uncollapsed areas of the lava tube, suggesting that the existence of skylights mainly reflects weakness zones and a higher degree of fracturing in the local in situ rock mass. This hypothesis is supported by numerical modeling where the implementation of a heterogeneous mechanical model of the lava tube, with reduced Young's modulus in the window areas, was crucial to reproduce field data. Moreover, numerical modeling allowed us to estimate the extent of the stiffness contrast between partly collapsed ($E_r = 2.4$ GPa) and intact portions ($E = 10$ GPa) of the roof.

Although Young's modulus values for intact basalt samples typically range from 35 to 85 GPa (Goodman 1989; Schultz 1993), when accounting for the effect of scale, rock mass deformation modulus reduces accordingly to the range of 5–40 GPa, for RMR and GSI between 45 and 75 (Schultz 1993, 1995; Blair et al. 2017). Our estimated value of 10 GPa for most areas of the lava tubes is thus well within the range of past in situ measurements of rock mass deformability (Schultz 1993). However, the rock mass around the lava tube skylights is, in particular, uniquely characterized by open fractures with large aperture in the range of 1–5 mm, further reducing rock mass modulus (Hoek et al. 2013). We can describe this as similar to excavation induced damage, and implement a disturbance factor (D) in the description of rock mass deformability (Hoek and Diederichs 2006). Assuming $D = 0.8$ (akin to poor quality blasting), rock mass deformation modulus decreases from 10 to 3 GPa, similar to our implemented value around the lava tube skylights. Moreover, while the Young's modulus obtained from our analysis of seismic data represent low-strain conditions (Barton 2007), they are similar to in situ experimental results of rock mass deformation testing (Schultz 1993). This finding was also described by Moore et al. (2018), who used similar field and numerical modeling techniques, that while strains resemble dynamic measurements, the resolved elastic moduli more closely resemble values from static measurements, being smaller than corresponding laboratory data. We hypothesize that measured modal deformations of the lava tube roof likely involve compliant opening and closing of rock mass discontinuities at multiple scales (and at scales appropriate for the investigated rock mass), making the deformability resolved from our analysis representative of a rock mass value.

Our modeling approach represents a simplified, continuum-based numerical modal analysis technique modeling jointed and fractured rock masses through a reduction of Young's modulus in discrete volumes. In contrast, several past studies have successfully modeled single, compliant and pervasive discontinuities by introducing planar surfaces (Colombero et al. 2017), open rear fractures (Guillemot et al. 2022), or boundary elements characterized by fixed or free

conditions (Bessette-Kirton et al. 2022). Here we used a simplified method suitable in geological applications for rock masses characterized by a high degree of fracturing (i.e., where the influence of single discontinuities cannot be easily discerned), in which the mechanical condition of a jointed rock mass can be approximated through the application of reduced-stiffness volumes (Burjánek et al. 2019).

The integrated approach applied in this study, combining ambient vibration array data and numerical eigenfrequency modeling, shows promising potential for mapping and structural characterization of underground cavities. As opposed to previous studies that mainly exploited ambient vibration measurements for subsurface imaging of karst systems (Nehme et al. 2013; Fedin et al. 2021), our results highlight that a similar methodology can be successfully applied for generalized characterization and structural health monitoring of underground cavity roofs in different geological contexts. While no inferences on the lava tube stability can be made from the obtained results, our approach can represent a benchmark in the perspective of replicating non-invasive field measurements after intense events (e.g., earthquakes or heavy rainfall), or periodically monitoring potential recoverable and permanent structural damage (Bessette-Kirton et al. 2022). For example, having identified the resonance modes of the Tabernacle Hill lava tube roof, it is now possible to perform periodic or long-term ambient vibration monitoring surveys to identify frequency drifts caused by progressive rock mass damage (Colombero et al. 2021; Geimer et al. 2022). Our integrated ambient vibration and numerical modeling approach could also find application in a broad range of other geological and cultural settings. In particular, this non-invasive methodology may be particularly useful for structural characterization and health monitoring of underground natural or cultural heritage sites in support of hazard assessment and conservation management.

Acknowledgements The authors thank Fan-Chi Lin and Elizabeth Berg for code used to conduct cross-correlation analyses, and the University of Utah Center for High Performance Computing for computational resources. Two anonymous reviewers provided valuable feedback that improved this manuscript.

Author Contributions Conceptualization: JRM, GG. Methodology: JRM, GG. Data collection and site investigation: GG, MEM, TLC, MMF, JRM. Data analysis: GG. Data interpretation: GG, JRM. Writing—original draft preparation: GG. Writing—review and editing: GG, JRM, EKJ, MEM. Funding acquisition: JRM. Resources: JRM. Supervision: JRM. All authors read and approved the final manuscript.

Funding This study was funded by the National Science Foundation (Grant No. 2150896).

Data Availability Datasets generated during the current study are available from the corresponding author on request.

Declarations

Conflict of interest The authors have no relevant financial or non-financial interests to disclose.

Open Access This article is licensed under a Creative Commons Attribution 4.0 International License, which permits use, sharing, adaptation, distribution and reproduction in any medium or format, as long as you give appropriate credit to the original author(s) and the source, provide a link to the Creative Commons licence, and indicate if changes were made. The images or other third party material in this article are included in the article's Creative Commons licence, unless indicated otherwise in a credit line to the material. If material is not included in the article's Creative Commons licence and your intended use is not permitted by statutory regulation or exceeds the permitted use, you will need to obtain permission directly from the copyright holder. To view a copy of this licence, visit http://creativecommons.org/licenses/by/4.0/.

References

Arisona A, Ishola KS, Muliddin M et al (2023) The potential of microgravity technique in subsurface cavities detection at Chan sow Lin site in Kuala Lumpur, Malaysia: a case study. Model Earth Syst Environ 9:771–782. https://doi.org/10.1007/s40808-022-01519-y

Barton N (2007) Rock quality, seismic velocity, attenuation and anisotropy. Taylor & Francis, London

Bastidas G, Soria O, Mulas M et al (2022) Stability analysis of lava tunnels on Santa Cruz Island (Galapagos Islands, Ecuador) using rock mass classifications: empirical approach and numerical modeling. Geosciences (switzerland). https://doi.org/10.3390/geosciences12100380

Bensen GD, Ritzwoller MH, Barmin MP et al (2007) Processing seismic ambient noise data to obtain reliable broad-band surface wave dispersion measurements. Geophys J Int 169:1239–1260. https://doi.org/10.1111/j.1365-246X.2007.03374.x

Bentivenga M, Capece A, Guglielmi P et al (2019) The San Giorgio Lucano anthropic cave complex (Basilicata, Southern Italy): a geosite to protect and enhance. Geoheritage 11:1509–1519. https://doi.org/10.1007/s12371-019-00374-1

Bessette-Kirton EK, Moore JR, Geimer PR et al (2022) Structural characterization of a toppling rock slab from array-based ambient vibration measurements and numerical modal analysis. J Geophys Res Earth Surf. https://doi.org/10.1029/2022JF006679

Blair DM, Chappaz L, Sood R et al (2017) The structural stability of lunar lava tubes. Icarus 282:47–55. https://doi.org/10.1016/j.icarus.2016.10.008

Burjánek J, Kleinbrod U, Fäh D (2019) Modeling the seismic response of unstable rock mass with deep compliant fractures. J Geophys Res Solid Earth 124:13039–13059. https://doi.org/10.1029/2019JB018607

Cardarelli E, Di Filippo G, Tuccinardi E (2006) Electrical resistivity tomography to detect buried cavities in Rome: a case study. Near Surf Geophys 4:387–392. https://doi.org/10.3997/1873-0604.2006012

Cardarelli E, Cercato M, De Donno G, Di Filippo G (2014) Detection and imaging of piping sinkholes by integrated geophysical methods. Near Surf Geophys 12:439–450. https://doi.org/10.3997/1873-0604.2013051

Colombero C, Baillet L, Comina C et al (2017) Characterization of the 3-D fracture setting of an unstable rock mass: from surface and seismic investigations to numerical modeling. J Geophys Res Solid Earth 122:6346–6366. https://doi.org/10.1002/2017JB014111

Colombero C, Baillet L, Comina C et al (2018) Integration of ambient seismic noise monitoring, displacement and meteorological measurements to infer the temperature-controlled long-term evolution of a complex prone-to-fall cliff. Geophys J Int 213:1876–1897. https://doi.org/10.1093/gji/ggy090

Colombero C, Jongmans D, Fiolleau S et al (2021) Seismic noise parameters as indicators of reversible modifications in slope stability: a review. Springer, London

Ebraheem MO, Ibrahim HA (2019) Detection of karst features using ground-penetrating radar: a case study from the western limestone plateau, Assiut, Egypt. Environ Earth Sci. https://doi.org/10.1007/s12665-019-8572-x

Esposito C, Belcecchi N, Bozzano F et al (2021) Integration of satellite-based A-DInSAR and geological modeling supporting the prevention from anthropogenic sinkholes: a case study in the urban area of Rome. Geomat Nat Haz Risk 12:2835–2864. https://doi.org/10.1080/19475705.2021.1978562

Fedin KV, Kolesnikov YI, Ngomayezwe L (2021) Mapping of underground cavities by the passive seismic standing waves method: the case study of barsukovskaya cave (Novosibirsk region, Russia). Geophys Prospect 69:167–179. https://doi.org/10.1111/1365-2478.13045

Finnegan R, Moore JR, Geimer PR et al (2022) Ground motion amplification at natural rock arches in the Colorado plateau. Seism Rec 2:156–166. https://doi.org/10.1785/0320220017

Geimer PR, Finnegan R, Moore JR (2020) Sparse ambient resonance measurements reveal dynamic properties of freestanding rock arches. Geophys Res Lett. https://doi.org/10.1029/2020GL087239

Geimer PR, Finnegan R, Moore JR (2022) Meteorological controls on reversible resonance changes in natural rock arches. J Geophys Res Earth Surf. https://doi.org/10.1029/2022JF006734

Goodman RE (1989) Introduction to rock mechanics, 2nd edn. Wiley, New York

Guillemot A, Baillet L, Larose E, Bottelin P (2022) Changes in resonance frequency of rock columns due to thermoelastic effects on a daily scale: observations, modelling and insights to improve monitoring systems. Geophys J Int 231:894–906. https://doi.org/10.1093/gji/ggac216

Hintz A (2008) Physical volcanology and hazard analysis of a young monogenetic volcanic field: black rock desert. Utah. MSc, University of South Florida

Hoek E, Diederichs MS (2006) Empirical estimation of rock mass modulus. Int J Rock Mech Min Sci 43:203–215

Hoek E, Carter TG, Diederichs MS (2013) Quantification of the geological strength index chart. In: 47th US rock mechanics/geomechanics symposium. ARMA, San Francisco, pp 1–8

Johnsen RL, Smith EI (2010) Subalkaline volcanism in the Black Rock Desert and Markagunt Plateau volcanic fields of south-central Utah

Kleinbrod U, Burjánek J, Fäh D (2019) Ambient vibration classification of unstable rock slopes: a systematic approach. Eng Geol 249:198–217. https://doi.org/10.1016/j.enggeo.2018.12.012

Liang D, Gan F, Zhang W, Jia L (2018) The application of HVSR method in detecting sediment thickness in karst collapse area of Pearl River Delta, China. Environ Earth Sci. https://doi.org/10.1007/s12665-018-7439-x

Lin FC, Li D, Clayton RW, Hollis D (2013) High-resolution 3D shallow crustal structure in long beach, California: application of ambient noise tomography on a dense seismic array. Geophysics. https://doi.org/10.1190/geo2012-0453.1

Liu R, Sun H, Qin J, Zheng Z (2023) A multi-geophysical approach to assess potential sinkholes in an urban area. Eng Geol. https://doi.org/10.1016/j.enggeo.2023.107100

Malinowska AA, Witkowski WT, Hejmanowski R et al (2019) Sinkhole occurrence monitoring over shallow abandoned coal mines with satellite-based persistent scatterer interferometry. Eng Geol. https://doi.org/10.1016/j.enggeo.2019.105336

Margherita Z, Claudio C, Laura E, Nocilla A (2018) A risk assessment proposal for underground cavities in hard soils-soft rocks. Int J Rock Mech Min Sci 103:43–54. https://doi.org/10.1016/j.ijrmms.2018.01.024

Moore JR, Geimer PR, Finnegan R, Thorne MS (2018) Use of seismic resonance measurements to determine the elastic modulus of freestanding rock masses. Rock Mech Rock Eng 51:3937–3944. https://doi.org/10.1007/s00603-018-1554-6

Müller J, Burjánek J (2023) In situ estimation of effective rock elastic moduli by seismic ambient vibrations. Int J Rock Mech Min Sci 170:105459. https://doi.org/10.1016/j.ijrmms.2023.105459

Nehme C, Voisin C, Mariscal A et al (2013) The use of passive seismological imaging in speleogenetic studies: an example from Kanaan Cave, Lebanon the use of passive seismological imaging in speleogenetic studies: an example from Kanaan Cave. Leban Int J Speleol. https://doi.org/10.5038/1827-806X.42.2.1ï

Oviatt CG (1991) Quaternary geology of the black rock desert, Millard county. Utah Geological and Mineral Survey Special Studies, Utah, p 73

Park MK, Park S, Yi MJ et al (2014) Application of electrical resistivity tomography (ERT) technique to detect underground cavities in a karst area of South Korea. Environ Earth Sci 71:2797–2806. https://doi.org/10.1007/s12665-013-2658-7

Pilecki Z, Krzysztof K, Elżbieta P et al (2021) Identification of buried historical mineshaft using ground-penetrating radar. Eng Geol. https://doi.org/10.1016/j.enggeo.2021.106400

Rao Y, Guo Y, Xu D (2021) Detecting karst voids based on dominant frequencies of seismic profiles. Pure Appl Geophys 178:3057–3067. https://doi.org/10.1007/s00024-021-02792-1

Schultz RA (1993) Brittle strength of basaltic rock masses with applications to Venus. J Geophys Res Planets 98:10883–10895. https://doi.org/10.1029/93JE00691

Schultz RA (1995) Limits on strength and deformation properties of jointed basaltic rock masses. Rock Mech Rock Eng 28:1–15. https://doi.org/10.1007/BF01024770

Theinat AK, Modiriasari A, Bobet A et al (2020) Lunar lava tubes: morphology to structural stability. Icarus. https://doi.org/10.1016/j.icarus.2019.113442

Waltham T (2008) Sinkhole hazard case histories in karst terrains. Q J Eng Geol Hydrogeol 41:291–300. https://doi.org/10.1144/1470-9236/07-211

Welch P (1967) The use of fast Fourier transform for the estimation of power spectra: a method based on time averaging over short, modified periodograms. IEEE Trans Audio Electroacoust 15:70–73. https://doi.org/10.1109/TAU.1967.1161901

Woo KS, Kim L, Ji H et al (2019) geological heritage values of the yongcheon cave (Lava Tube Cave), Jeju Island, Korea. Geoheritage 11:615–628. https://doi.org/10.1007/s12371-018-0315-y

Publisher's Note Springer Nature remains neutral with regard to jurisdictional claims in published maps and institutional affiliations.